Polymer Degradation and Stability 210 (2023) 110295

Contents lists available at ScienceDirect

Polymer Degradation and Stability

journal homepage: www.journals.elsevier.com/polymer-degradation-and-stability

Enhanced photocatalytic degradation of PE film by anatase/γ-MnO_2

Iryna Kovinchuk [a], Nadiia Haiuk [b,c], Giuseppe Lazzara [d], Giuseppe Cavallaro [d,*], Georgii Sokolsky [a,c,**]

[a] National Technical University of Ukraine "Igor Sikorsky Kyiv Polytechnic Institute" Faculty of Chemical Technology, 37, Peremohy ave., Bldg 4, Kyiv 03056, Ukraine
[b] Bila Tserkva National Agrarian University, Soborna Square, 8/1, Bila Tserkva 09117, Ukraine
[c] Department of Physics and Chemistry "E. Segrè", University of Palermo, Viale delle Scienze, pad. 17, Palermo 90128, Italy
[d] Department of Chemistry and Chemical Technology, National Aviation University, Lubomyr Guzar avenue, 1, Kyiv 03058, Ukraine

ARTICLE INFO

Keywords:
Polyethylene film
Photocatalytic degradation
Manganese dioxide
Titanium dioxide

ABSTRACT

The photocatalytic degradation of low-density polyethylene (PE) films containing nanoparticles (NP) of titanium and manganese dioxides has been investigated. Composite PE films were prepared by the casting of p-xylene with the photocatalyst (TiO_2, MnO_2 or hybrid 1: 1 TiO_2&MnO_2) content of 1 wt%. The polyethylene degradation test has been carried out in a photoreactor with UV-irradiation (Hg lamp). Then, FTIR spectroscopy and gravimetric measurements have been conducted after the UV exposure at variable time to evaluate the NPs photocatalytic effects within the PE matrix. According to these tests, we detected the coupling effects of TiO_2 and MnO_2 nanoparticles on the PE photo-degradation. Moreover, the influence of TiO_2 and TiO_2&MnO_2 on the tensile properties, thermal behavior under inert atmosphere and wettability characteristics of PE based films have been explored by DMA, TGA and water contact angle measurements, respectively. Based on TGA data, we studied the effects of TiO_2 and TiO_2&MnO_2 nanoparticles on the kinetics of the PE thermal degradation.

1. Introduction

Polyethylene (PE) waste disposal is a crucial problem that causes severe issues to the environment. Photocatalytic degradation of PE is a promising method to reduce the amounts of pollutants. In this regard, titanium dioxide (TiO_2) is widely used for the photocatalytic degradation of PE environmental pollutants [1–3] due to its remarkable photocatalytic activity, physical and chemical stability, low cost, non-toxicity, and large distribution in nature [4–6].

Photocatalytic activity depends on the ability of the catalyst to create electron-hole pairs, which generate free radicals that can take part in secondary reactions. This ability is defined directly by the band gap of the semiconductor. TiO_2 has a high photoactivity with a band gap of 3.2 eV (for anatase), 3.0 eV (for rutile), 3.4 eV (for brookite) [7,8]. These values of the band gap indicate the beginning of the photoreaction at a wavelength of less than 400 nm. When TiO_2 is excited by photons with energy higher than its band gap energy level, electrons from the valence band can move to the conduction band and generate electron-hole pair that can participate in reductive (electron) or oxidative (hole) processes.

Since only 5–8% of the solar spectrum is UV radiation, photocatalytic degradation under visible light is crucial to use more solar energy. To increase the photocatalytic activity under visible light, it is necessary to reduce the value of the band gap of the catalyst. It can be achieved by increasing the concentration of defects of the crystals, by modifying the synthesis process or by doping with noble or transition metals, as well as compounds of Cd, Zn, Cu, Pb, Fe, Mo [9–12].

Among various semiconductor materials, MnO_2 seems to be particularly attractive due to its non-toxicity, low cost, and wide abundance in nature. It is widely used as an oxidant to oxidize volatile organic compounds (VOC) [13]. Moreover, literature showed that the MnO_2 activity is comparable to that of noble metals for the conversion of CO to CO_2 [14]. The evidence of photocatalytic behavior of MnO_2 has been recently demonstrated [15].

The photocatalytic activity of MnO_2/TiO_2 composite for water purification was studied by L. Zhang et al. [16]. Furthermore, the effect of TiO_2 on the oxidative activity of MnO_2 was described by S.Taujale and H. Zang [17].

An increase in the available surface of the catalyst contributes to the

* Corresponding author.
** Corresponding author at: National Technical University of Ukraine "Igor Sikorsky Kyiv Polytechnic Institute" Faculty of Chemical Technology, 37, Peremohy ave., Bldg 4, Kyiv 03056, Ukraine.
E-mail addresses: giuseppe.cavallaro@unipa.it (G. Cavallaro), georgii.sokolsky@gmail.com (G. Sokolsky).

https://doi.org/10.1016/j.polymdegradstab.2023.110295
Received 14 October 2022; Received in revised form 10 February 2023; Accepted 12 February 2023
Available online 15 February 2023

rapid rate of surface reactions and enhancement of photocatalytic reactions [18,19]. The undoubted advantage of nanoparticles compared to larger particles is the maximum probability of release of separated charges on the catalyst surface and the minimum - of their recombination, respectively. Due to the fact that the depth of penetration of UV light into TiO_2 particles is limited (~ 100 nm) [20] reducing particle sizes to nanoscale values helps absorb light throughout the titanium dioxide volume. Therefore, the use of nanopowders is optimal in the processes of heterogeneous photocatalysis.

To provide the "coupling" effect of TiO_2 with MnO_2 and shifting the activity of the photocatalyst in the visible range, it is essential to ensure maximum homogenization. As reported in literature [21], the uniform distribution of composite oxide materials throughout the film is an important condition. A special preparation procedure for polyethylene film is necessary. In addition, to compare the photocatalytic activity of samples, investigations of the film mass loss under UV-irradiation should be studied.

The aim of this study is to investigate the properties of PE films with photocatalytic additives and the efficiency of photocatalytic degradation of PE/TiO_2, PE/TiO_2&MnO_2 films under UV-irradiation to confirm the hypothesis about the possibility of the coupling effect of titanium dioxide photocatalyst combined with a semiconductor having the narrower forbidden band.

It is worth noting the data of the EU report on the possible disadvantages of using polyethylene with the addition of a photocatalyst. Namely, the impossibility of disposal through composting, difficulties in the process of secondary processing associated with sorting, the formation of microplastic particles that can easily spread with wind and water, polluting the environment Nevertheless, the PE utilization problem is of crucial importance that requires new practice-oriented approaches.

Prior to the photodegradation tests, we studied the properties of nanocomposite films based on PE and inorganic nanocatalysts (TiO_2 and TiO_2&MnO_2) in terms of tensile performances and thermal stability, which were investigated by the combination of thermal analyses techniques largely employed in the characterization of polymer/nanofiller hybrid materials [22–32]. Moreover, we investigated the wettability characteristics of the composite films by water contact angle measurements.

2. Experimental

2.1. Materials

Granules of pure low-density polyethylene (LDPE) 15,803–020, p-xylene (Russia), MnO_2 of industrial production (Prydniprovsky Chemical Plant, Kamyanske, Ukraine); TiO_2 (anatase) produced by Institute for Problem of Material Science of NASU were used. All these reagents were at least of chemically pure grade.

2.2. Preparation of the films

The film preparation (Fig. 1) process was adapted from [33] in which granules of 0.5 g of PE were added to 25 ml of p-xylene, then heated in an oven at 110 °C for 40–45 min. After PE melting, inorganic components, namely pure TiO_2, and the mixture of TiO_2 and MnO_2 (1:1) were added at a concentration of 1 wt%. Ultrasonic stirring was applied in the ultrasonic bath BK-9050 (Baku, China) filled with distilled water. The time of processing was not less than 60 min, the power was 50 W.

Afterwards, the dispersions were poured into a glass Petri dish (9 cm in diameter). Finally, the solvent casting method was carried out at a temperature of 110 °C to obtain a film that delaminates the glass dish easily. The same procedure was applied to prepare a film of pure PE dissolved in p-xylene. The average thickness of the resulting PE-composite film was 50–70 μm.

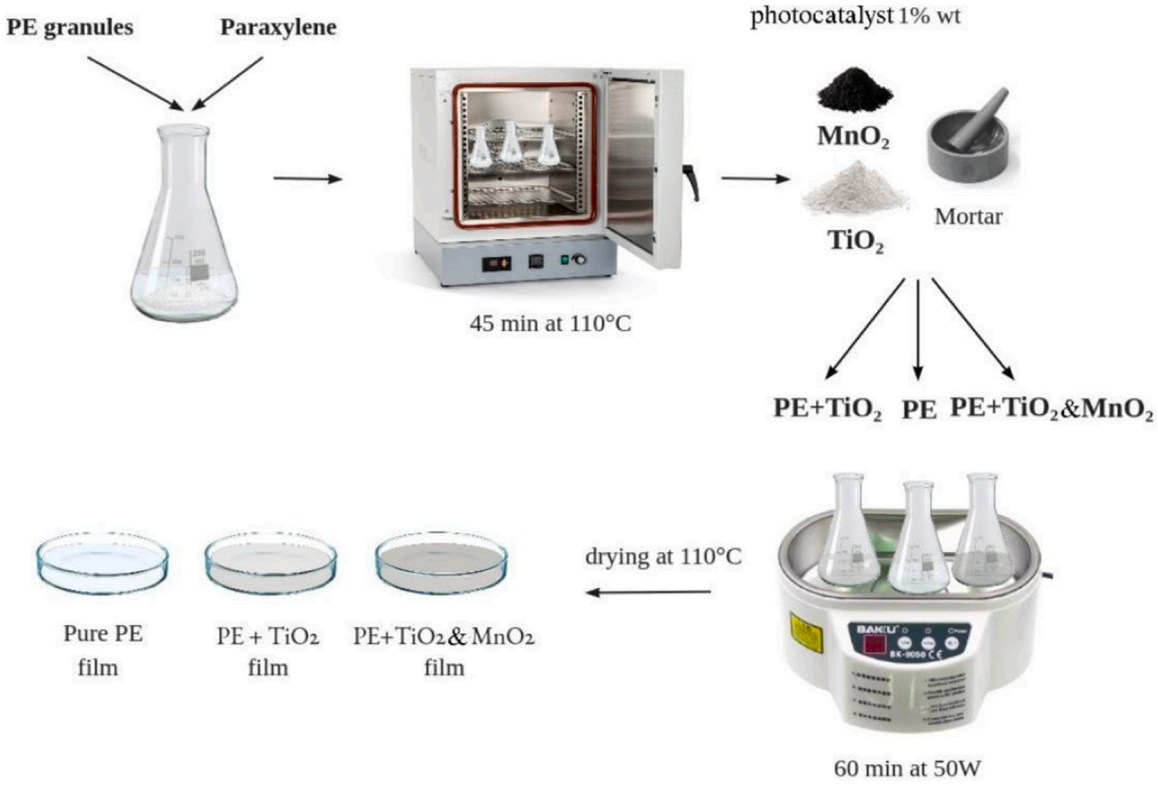

Fig. 1. Preparation protocol of the nanocomposite films.

3. Methods

3.1. Water contact angle measurements

Contact angles were studied using an optical contact angle apparatus (OCA 20, Data Physics Instruments) equipped with a high-resolution CCD camera. The SCA 20 (Data Physics Instruments) software was used for data collection and analysis. Rectangular (7 × 20 mm) films were fixed on top of a plane solid support with double-sided tape. The contact angle (θ) of water in the air was measured using the sessile drop method by placing a droplet of 10.0 ± 0.5 μl onto the surface. The temperature was set at 25.0 ± 0.1 °C for the support and the injecting syringe as well. Images were collected at a rate of 50 frames per second. A minimum of 2 droplets were examined for each film sample.

3.2. Dynamic mechanical analysis (DMA)

Dynamic mechanical measurements were conducted using the DMA Q800 (TA Instruments). Tensile tests were performed with a stress ramp of 1 MPa·min^{-1} at 25.0 ± 0.5 °C. The values of the elastic modulus, the tensile strength (defined as the tensile stress at which the sample starts to form fractures), the percent elongation at the break and yield point of films were also determined.

3.3. Thermogravimetric analysis (TGA)

Thermogravimetric Analyzer Discovery TGA550 with TRIOS Software was applied. Measurements were carried out under the nitrogen flow of 60 cm^3 min^{-1} for the sample and 40 cm^3 min^{-1} for the balance. The temperature range was between 25 and 600 °C. Each sample was placed in a platinum pan and heated under the modulate temperature of 5 °C min^{-1} for 200 s. Then, a heating ramp of 2 °C min^{-1} was applied up to 600 °C. The processed experimental data allowed us to determine the decomposition temperature (T_d) taken at the peak of the differential thermogravimetric (DTG) curves and the activation energy. The QtiPlot software was used for the treatment of the TG data.

3.4. FTIR-spectroscopy

FTIR spectra of pure PE films and films with photocatalysts were studied with different time of UV-exposition. FTIR spectrometer FSM-1201(Infraspek, Russia) with a spectral resolution of 1 cm^{-1} over the range of 4000–500 cm^{-1} with 20 scans per spectrum was applied. Indexes of some functional groups were calculated from the ratio of the height of their characteristic band and the reference peak of rotational vibration of CH_2 groups 720 cm^{-1} which was not affected by degradation process and well isolated from other peaks [34].

3.5. Treatment of films by UV-irradiation

The irradiation source was an ultraviolet lamp OUFK - 01. Samples were irradiated under a 6 W ultraviolet lamp at ambient air and temperature in a lamp-housing box (50 cm • 40 cm • 30 cm). The wavelength distribution of the lamp was about 280 nm. The samples were placed at a distance of 5 cm from the irradiation source. Irradiation was carried out at regular intervals of 10 h. To control mass loss, films were weighed on an analytical balance XAC 220/C with an accuracy of 0.0001 g.

3.6. Scanning electron microscopy analysis

SEM analysis was carried out in high vacuum 10^{-1} - 10^{-2} Pa by means of Tescan Mira 3 LMU microscope (Czech Republic). The energy of the beam was set at 10 kV, while the working distance was fixed at 1.98 mm.

4. Results and discussion

Based on the statistical analysis of SEM images (Fig. 2) using ImagJ and SciDAVi softwares, we estimated that the average size of MnO_2 nanoparticles is 40 ± 5 nm, while the average size of TiO_2 nanoparticles is 20 ± 5 nm as reported elsewhere [35].

MnO_2 NPs are formed by the aggregated needle-like crystallites with an average length of 200–1000 nm, It is worth noting that BET surface area of manganese dioxide is relatively low (20–30 m^2/g). NPs of anatase TiO_2 have no regular shape and are smaller than MnO_2 NPs.

4.1. Wettability and tensile performance of the nanocomposite films

Fig. 3 shows the photos and the corresponding contact angle values for the water droplets immediately after their deposition on PE, PE/TiO_2 and PE/TiO_2&MnO_2 films. As a general result, the contact angle values are close to 90° indicating that the surface films is hydrophobic. We observed that the presence of the inorganic fillers does not significantly affect the wettability of PE. The slight hydrophobization of the surface in the composite materials may be attributed to the increased surface roughness.

The effect of the nanofiller addition on the tensile properties of PE based films was studied by DMA experiments. The obtained stress vs strain curves are displayed in Fig. 4, while the related tensile parameters are reported in Table 1.

According to literature [36], the addition of the nanoparticles caused a decrease of the ultimate elongation. This effect could be attributed to the PE/nanofillers interactions, which prevent the sliding between the polymeric chains [37]. Oppositely, the PE filling with TiO_2 improved the elastic modulus and the stress at the breaking point, while the presence of TiO_2&MnO_2 did not generate any significant variations on these parameters.

4.2. Thermal behavior of the nanocomposites under inert atmosphere

We investigated the thermal properties of pristine PE and the nanocomposites (PE/TiO_2 and PE/TiO_2&MnO_2) by thermogravimetric experiments performed under Nitrogen flows, which guarantee an inert atmosphere. Within this, it should be noted that thermogravimetry under inert gas flows is suitable to explore the thermal characteristics of nanocomposite films obtained by the filling of polyethylene matrix with nanoparticles [38,39]

Fig. 5 shows the thermogravimetric (TG) and differential thermogravimetric (DTG) curves of PE based films.

As shown in Table 2, we detected that the residual masses at 575 °C (RM_{575}) are higher in the composites with respect to that of pristine PE. These results are consistent with the incorporation of the inorganic nanofillers within the polymeric matrix. As a general result, the TG curves show a significant decrease in the temperature range between ca. 250 and 500 °C that reflects the thermal degradation of the polymer. The PE degradation temperature (T_d) was calculated from the minimum of the DTG peaks (see insets in Fig. 5). We observed that the T_d values of PE and PE/TiO_2&MnO_2 are similar (442 and 444 °C, respectively), whereas the addition of TiO_2 generated a reduction of the polymer degradation temperature being that the T_d of PE/TiO_2 is 434 °C.

Moreover, we studied the influence of the nanoparticles (TiO_2 and TiO_2&MnO_2) on the kinetics of the PE thermal degradation. In this regard, the ICTAC Kinetics Committee evidenced that thermogravimetry is a suitable technique to determine the kinetic parameters (activation energy and pre-exponential factor) related to the thermal degradation of polymer and polymer/filler composites [40]. On this basis, we estimated the activation energy (E) and the pre-exponential factor (A) in the interval 250–500 °C to explore the influence of the nanofillers on the kinetics of the PE degradation. Table 2 reports the average values for both kinetic parameters. We observed that the presence of the nanofillers slightly reduces the activation energy of the PE degradation indicating

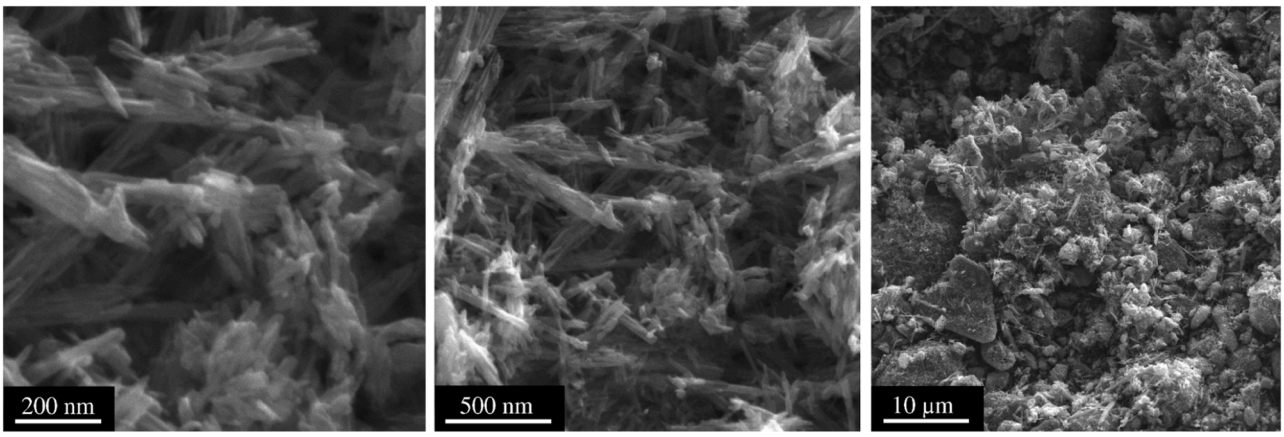

Fig. 2. SEM images of pure MnO_2 nanoparticles.

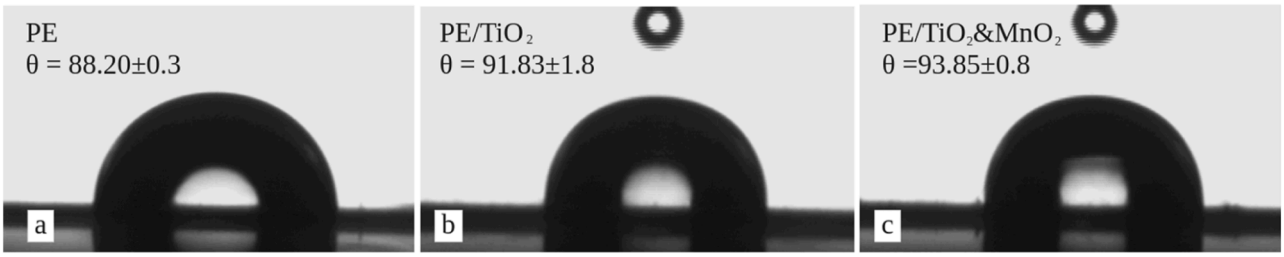

Fig. 3. Images of water droplets and the corresponding contact angle values just after their deposition on the surface of (a) PE, (b) PE/TiO_2, (c) PE/TiO_2&MnO_2.

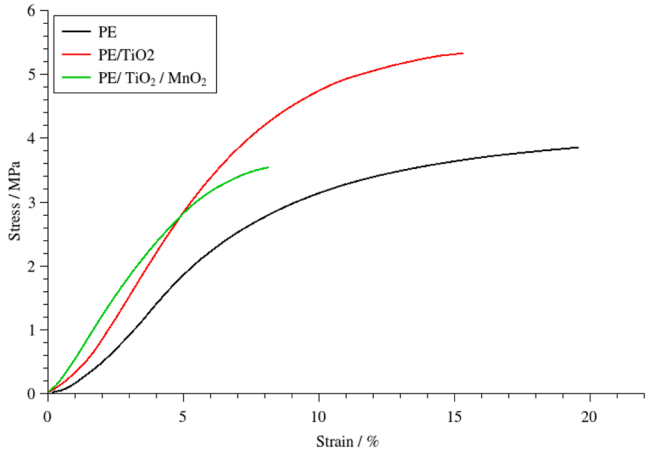

Fig. 4. Stress versus strain curves for pure PE, composite films PE/TiO_2 and PE/TiO_2&MnO_2.

that both TiO_2 and TiO_2&MnO_2 enhance the energetic barrier to the thermal decomposition of the polymer.

According to the ICTAC Kinetics Committee recommendations [40], we analyzed the TG data at 250–500 °C by Master plots to determine the reaction model of the PE degradation. We detected that the PE degradation process can be described by the Avrami–Erofeev model (code A3) for all samples. As reported in numerous studies [40–42], the determination of the kinetic triplet (activation energy, pre-exponential factor and reaction model) allows us to predict the time dependence for thermal degradation of organic macromolecules, including polymers. In particular, we can calculate the time (t_α) required to achieve a certain conversion degree (a) of degradation at a fixed temperature (T_0) by using the following equation:

$$t_\alpha = \frac{g(\alpha)}{A exp\left(\frac{-E}{RT_0}\right)} \quad (1)$$

where $g(\alpha)$ is the integral form of the reaction model. As concerns the A3 model, $g(\alpha)$ is expressed as $[-\ln(1-\alpha)]^{1/3}$.

According to the Eq. (1), we can determine the t_a vs a functions at under isothermal conditions at variable temperature. These trends represent the simulations of the PE conversion degree over time allowing us to the explore the effect of the addition of the nanofillers on the thermal degradation of the polymer. In this regard, literature reports that the lifetime of polymeric materials can be estimated when a conversion degree equals to 0.05 is reached [40,41,43]. Namely, ICTAC recommendations report that the limiting extent of decay beyond which the material becomes unusable can be defined when 5% mass loss is reached [40]. Nevertheless, it should be noted that TGA is a high risk approach for any polymer lifetime predictions because the thermogravimetric experiments tend to focus on degradation chemistry pathways irrelevant for the usual applications [44]. A more accurate estimation of the polymer lifetime needs to establish the correlation between

Table 1
Tensile properties of PE, PE/TiO_2, and PE/TiO_2&MnO_2 films.

	Elongation at break /%	Stress at break point / MPa	Elastic modulus / MPa	Yield point /%
PE	21.91	3.93	61.40	7.56
PE/TiO_2	14.19	5.27	82.08	7.64
PE/TiO_2&MnO_2	8.1	3.54	63.49	5.42

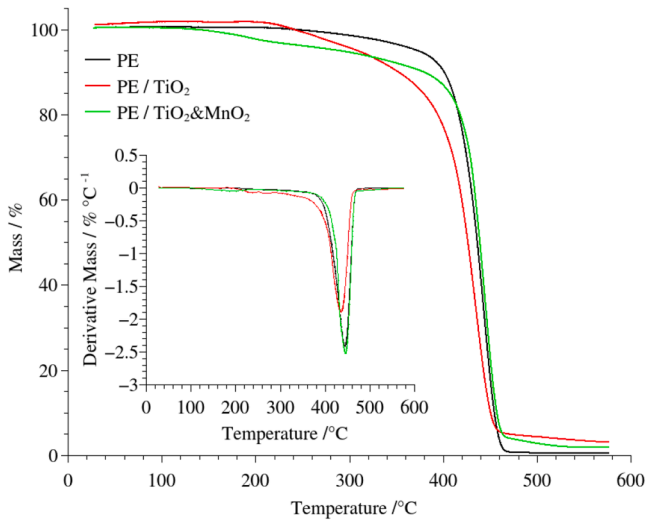

Fig. 5. TG curves of PE, PE/TiO_2, and PE/TiO_2&MnO_2. Inset: corresponding differential thermogravimetric curves.

degradation chemistry and materials performance, which is generally associated to mechanical properties (elasticity, toughness, adhesion, impact fracture resistance). Furthermore, changes on the molecular weight and other attributes, such as transmissivity and discoloration, can be appropriate to predict the progressive material degradation of polymers.

Fig. 6 shows the simulated t_a vs a curves for pristine PE and the nanocomposites at four different temperatures (250, 300, 400 and 500 °C) within the interval of the polymer degradation.

Based on the quantitative analysis of these curves, we determined the t_a required to achieve a = 0.05 (Table 3). These values are related to the thermal resistance of PE under inert atmosphere ruling out any potential effects (such as polymer embrittlement) due to oxidative [44] and hydrolytic reactions [45].

As general result, PE/TiO_2nanocomposite exhibited the lowest t_a(a = 0.05) value highlighting that the presence of TiO_2 nanoparticles favor the thermal decomposition of the polymer. On the other hand, the influence of TiO_2&MnO_2 on the PE thermal stability depends on the temperature. Compared to the pristine polymer, we determined that the PE filling with TiO_2&MnO_2 generates a reduction of the t_a(a = 0.05) value at 250 and 300 °C. Oppositely, PE/TiO_2&MnO_2 showed the largest t_a(a = 0.05) values at higher temperatures (400 and 500 °C) evidencing that the addition of the mixed nanofillers (TiO_2&MnO_2) increased the thermal stability of the polymer.

4.3. Photodegradation of composite films: Mass loss measurements and FTIR investigations

Photos of films after UV-irradiation are shown in Fig. 7. It is evident that under UV-irradiation the mechanical mixture of TiO_2 with MnO_2 has significantly more pronounced effect as a photocatalyst than pure TiO_2. With a total UV-irradiation of about 90 h, there is a synergistic increase in mass loss of the film with a mixture of 1:1 TiO_2&MnO_2 (21.2 wt%) compared to films with photocatalyst based on individual TiO_2 (14.6 wt%) component (Fig. 8a).

Coupling effect of TiO_2 with MnO_2 probably explains the synergism

Table 2
Thermal parameters of PE, PE/TiO_2, and PE/TiO_2&MnO_2 films.

Sample	RM $_{575}$ /%	T_d / °C	Activation energy / kJ mol^{-1}	Pre-exponential factor / s^{-1}
PE	0.62	442	213 ± 21	(468 ± 10) • 10^{10}
PE/TiO_2	3.18	434	201 ± 15	(936 ± 12) • 10^{9}
PE/TiO_2&MnO_2	1.94	444	203 ± 14	(605 ± 9) • 10^{9}

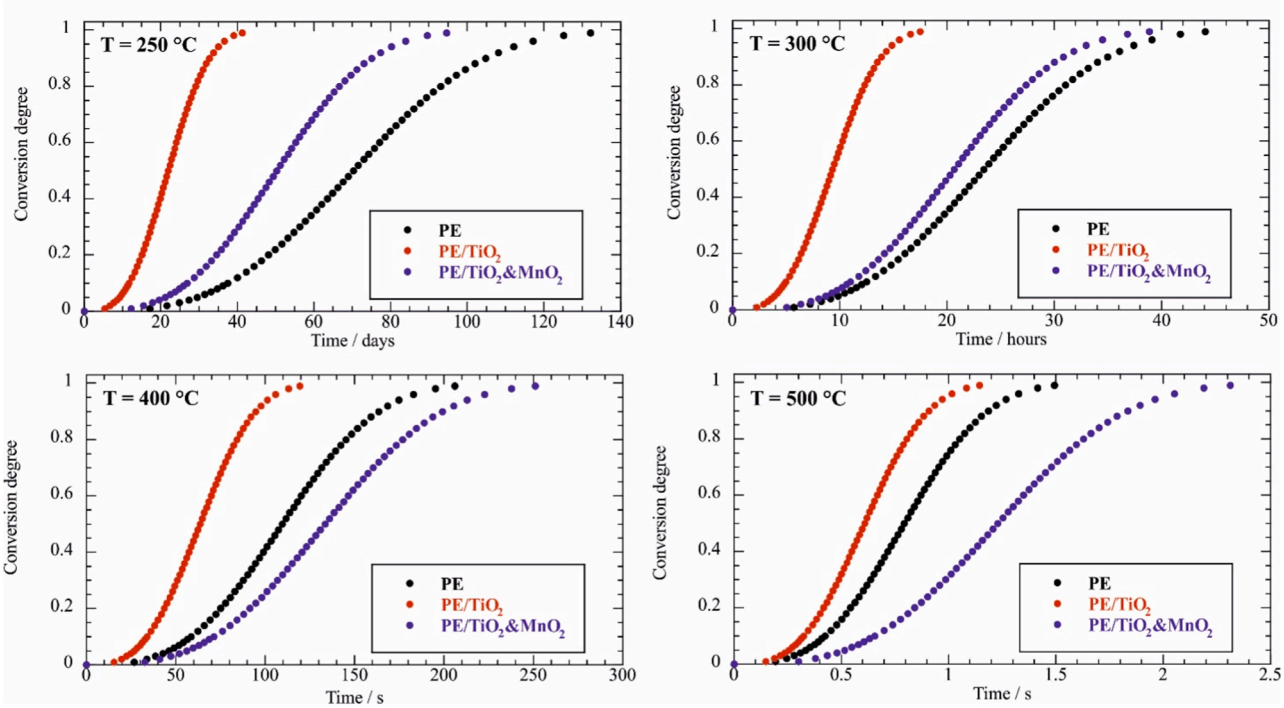

Fig. 6. Simulated t_a vs a curves under isothermal conditions at variable temperatures (250, 300, 400 and 500 °C) for PE, PE/TiO_2, and PE/TiO_2&MnO_2.

Table 3
Time (t_α) required to achieve a 0.05 conversion degree for thermal degradation of PE, PE/TiO_2 and PE/TiO_2&MnO_2 under inert atmosphere at 250, 300, 400 and 500 °C.

Sample	t_α (α=0.05) 250 °C	t_α(α=0.05) 300 °C	t_α(α=0.05) 400 °C	t_α(α=0.05) 500 °C
PE	29.5 days	9.84 h	42.03 s	0.336 s
PE/TiO_2	8.53 days	3.91 h	24.71 s	0.255 s
PE/TiO_2&MnO_2	21.13 days	8.67 h	56.06 s	0.516 s

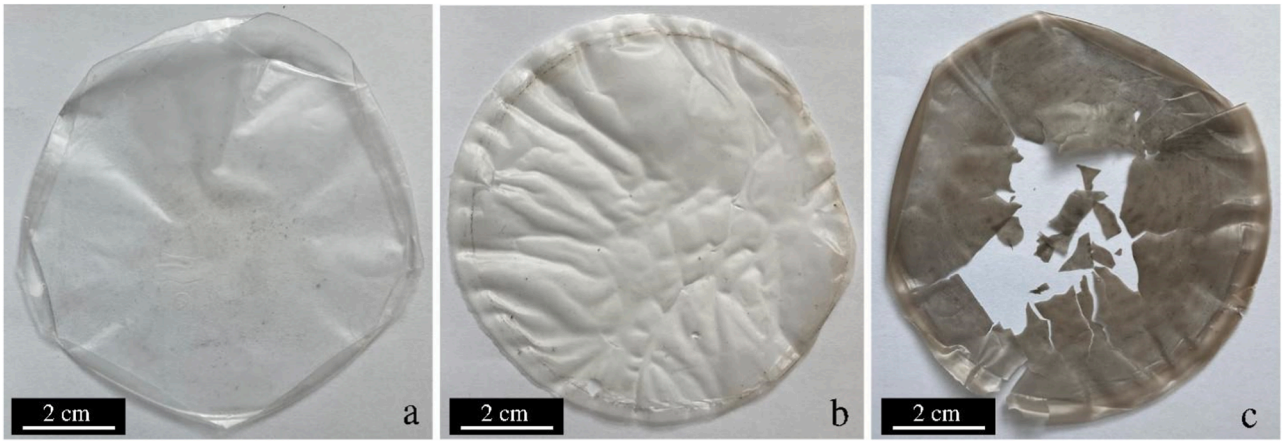

Fig. 7. Images of PE (a), PE/TiO_2 (b), PE/TiO_2&MnO_2 (c) films after 90 h of UV-irradiation.

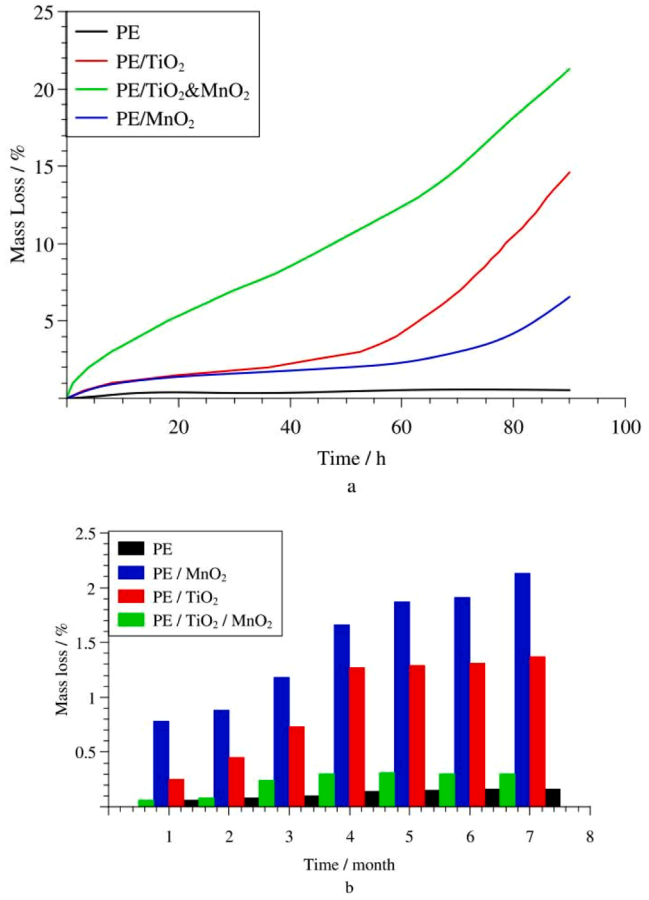

Fig. 8. Profile of mass loss of films as a function of irradiation time in the presence of photocatalysts (a); chart of mass loss of the films in dark conditions (b).

of the simultaneous action of both oxides. Thus, the reason for the increase in mass loss may be the improved separation of photoinitiated charge carriers in the presence of manganese dioxide. Therefore, the use of nanosized TiO_2 with MnO_2 leads to a significant increase in photocatalytic activity.

Fig. 8b shows the results of mass loss by films in the dark. Rutile polymorph of titanium dioxide was used in this experiment. Both anatase and rutile have no oxidizing and photocatalytic properties at these conditions. Since titanium dioxide is a photocatalyst, it performed worse than manganese dioxide in the absence of light. As expected, manganese dioxide showed a better result due to its oxidizing properties. The drastic decrease in the effectiveness of TiO_2&MnO_2 mixture can be explained by blocking the polymer degradation process by manganese dioxide reduction products.

The FTIR spectrum of the pure film contains active bands at 2920 and 2850 cm^{-1} of the asymmetric and symmetric -CH_2 groups stretching vibrations, respectively (Fig. 9). The intense band at 1467 cm^{-1} corresponds to the deformation vibration of the CH_2-group. The band at 727 cm^{-1} belongs to the absorption band of γ-fluctuations of the CH_2-group. Their positions remain constant in the process of degradation.

Irradiated films show new absorption bands that are particularly intense for a sample PE/TiO_2&MnO_2. A wide band at 3400 cm^{-1}, a sharp band at 1720 cm^{-1}, and a wide complex area of 800–1400 cm^{-1} are of maximum intensity. Some of the available absorption bands correspond to alcohols: the bound OH-group vibration occurs as a wide IR band above 3400 cm^{-1}, the in-plane bending or deformation of OH-group at 1200 - 1450 cm^{-1}, and the stretching band of C – O group between 970 and 1260 cm^{-1}. Usually, the position of these frequencies varies as follows: CH_2—OH - 1075–1000 cm^{-1}; CH—OH 1125–1000 cm^{-1}; C—OH 1210 - 1100 cm^{-1} [43]. The strong absorption band at 1720 cm^{-1} belongs to the stretching vibrations of the C = O functional group. The available data suggests more in favour of the ketone carbonyl compared to the carboxyl group. First, there is bonded OH-group at 3200–3300 cm^{-1} without narrow band of free OH carboxyl group at 3500–3550 cm^{-1}. Secondly, it is impossible to clearly record the out-of-phase bending of OC-OH at 880–960 cm^{-1}.

Nature of the effects on the FTIR spectra of oxide-modified films is complex. Esters are also possible products with two strong bands of

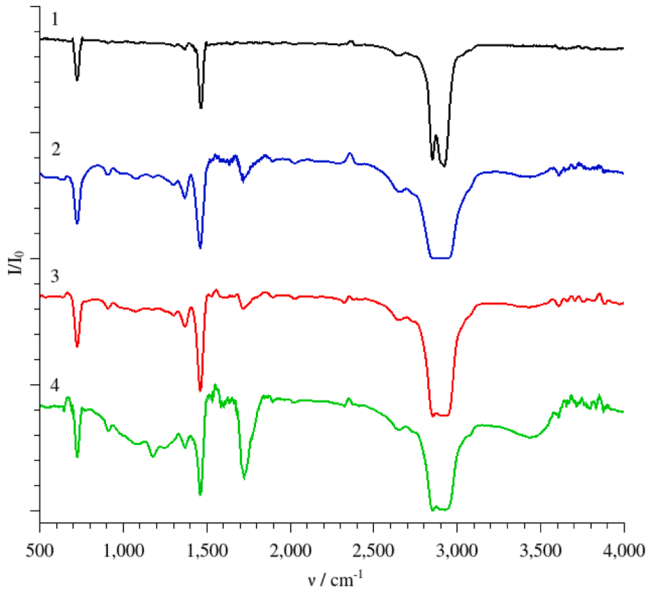

Fig. 9. FTIR spectra of films: 1 - PE before irradiation; 2 - PE after 40 h of UV; 3 - PE/TiO_2 after 40 h of UV; 4 - PE/TiO_2&MnO_2 after 40 h of UV.

symmetric and asymmetric stretching vibrations of C – O in the range of 1050 - 1300 cm^{-1}. Formates and propionates (1185 cm^{-1}), acetates (1240 cm^{-1}), γ- and δ-lactones (1180 cm^{-1}) are quite possible candidates for asymmetric stretching vibration [43].

As reported elsewhere [46], the intensive absorption band between 3150 and 3550 cm^{-1} may be explained by hydroperoxide group formation.

The oxygen-containing groups formed during PE-film degradation should increase the sample's mass. However, the kinetic curves demonstrate mass loss clearly. It points out the probable formation of facilitated by catalyst intermediates in the near-interface region of alcoholic OH-groups with further oxidation to ketone carbonyls, which, in turn, are able to further interact with the formation of esters when the C–C bonds are broken. The last step includes the cleavage of CO_2 and the further decomposition of formates and acetates. Therefore, the list of compounds may not be complete.

The degradation of a PE film modified with TiO_2 is not only the photolytic reaction of PE, but also the photocatalytic reaction of PE on the surface of the photocatalyst. A possible degradation mechanism has been described in literature [46–49]. It includes formation of holes and electrons reacting with LDPE and through macromolecular radicals producing superoxide anion and hydroxyl radical which are highly reactive oxygen species for the degradation of PE

As reported in [15], after 288 h of UV irradiation of PE/α-MnO_2 (cryptomelane-type) there were new absorption peaks at 1713 cm^{-1} and 1177 cm^{-1}, which correspond to the C = O and C—O stretching vibrations. They are also present in the obtained spectra of PE/TiO_2&MnO_2 (ramsdellite-type) composite film. This observation for PE/α-MnO_2 and PE/TiO_2&γ-MnO_2 could refer to the same degradation mechanism for different MnO_2-polymorph containing PE films.

The carbonyl index (CI) is often used to assess the degree of photo-oxidation of the polyethylene [50]. The same approach can be applied to other functional groups of degradation intermediates like hydroxyls (HI) or, for instance, to a new functional group absorption band of degradation product at 1177 cm^{-1}(NI) that could be assigned to C—O stretching vibrations. CI & HI of different PE films were obtained by normalizing the characteristic C = O band at 1720 and OH stretching vibration band at 3430 cm^{-1} with respect to 720 cm^{-1} isolated band of PE [44,51–53]. NI was calculated by a similar procedure. The calculated data for investigated samples are presented in Table 4, which shows that the addition of TiO_2/MnO_2 caused relevant changes on the CI, HI and NI

Table 4
Functional groups indexes (CI, HI, NI) related to the degradation products.

	CI / arb. Units (1720/720)	HI /arb. units (3430/720)	NI /arb. units (1175/720)
PE before UV	0.13	0.19	0.14
PE after UV	0.36	0.31	0.32
PE/TiO_2	0.34	0.31	0.36
PE/ TiO_2&MnO_2	1.27	0.73	0.99

indexes. The slight deviations of indexes for PE/TiO_2 film vs pure PE film after UV-exposition as well as PE/TiO_2&MnO_2 film behavior are the signatures of the different photo-oxidation mechanisms. The identical indexes of PE/TiO_2 and PE after UV with a simultaneous significant difference in the mass loss (Fig. 8a) demonstrate the nature of the limiting stage in the process. Probably, anatase TiO_2 is a photocatalyst of the last CO_2 cleavage stage attended by the C—C bond breakage. The possible TiO_2&MnO_2 (ramsdellite-type) coupling effect explanation using FTIR and photodegradation mass loss data could be the following: γ-MnO_2 nanoparticles combined with TiO_2 are more active in intermediate steps of PE oxidation that is why intermediates' functional groups are more accumulated comparing with PE/TiO_2 -film.

A graphical analysis of the kinetic dependence of the mass loss of composite films on the irradiation time was carried out. An equally high correlation coefficient was found for the dependence of zero and first orders for the PE/TiO_2&MnO_2 sample. The same behavior is typical for samples with individual TiO_2 in the early stages of degradation. This allows us to conclude that the composite catalyst stabilizes a definite degradation mechanism.

The theoretical models of chemical solid-phase reactions were tested using Yander's, Anti-Yander's, and Wagner's equations [54]. According to the Erofeev-Avrami equation, the nuclear model demonstrated the best correspondence for sections of curves where the kinetic dependences of the 0th and 1st order are fulfilled. Thus, the nuclei of oxidation products are grains rather than flat ($n = 2, 3$). Such a reaction is likely to occur in a heterogeneous region and therefore has a zero order.

5. Conclusions

We prepared nanocomposite films obtained by the filling of low-density polyethylene (PE) matrix with TiO_2 as well as with TiO_2&MnO_2. The films were prepared by the casting of PE in p-xylene. The filler concentration was kept constant at 1 wt%. We detected that the PE filling with TiO_2&MnO_2 generates a slight hydrophobization of the polymeric film, while the highest improvements of the tensile performances were achieved by adding pristine TiO_2 nanoparticles. Thermogravimetric experiments under inert atmosphere showed that the TiO_2 nanoparticles enhance the kinetics of the PE thermal decomposition for any temperature within the interval ranging between 250 and 500 °C. On the other hand, the influence of the TiO_2&MnO_2 composite nanofiller depends on the specific temperature. We observed a stabilization effect on the PE thermal resistance at 400–500 °C, while opposite results were estimated for lower temperatures (250–300 °C).

We investigated the photocatalytic degradation of PE films containing nanoparticles of titanium and manganese dioxides. The photodegradation results evidenced the coupling effects between TiO_2 and MnO_2 semiconductors. The most intensive and distinctive view of absorbance of oxygen-containing species of alcohols, ketones, and esters on FTIR spectra is inherent to PE/TiO_2&MnO_2 film. In addition, the mass loss features of studied films are in favour of additional mechanisms that facilitate the complete degradation process for PE/TiO_2&MnO_2 film. The latter exhibits the best degradation result with a mass loss of about 21.3% after 90 h of UV irradiation.

We observed that the presence of γ-MnO_2 photocatalyst generates an

identical PE degradation mechanism with respect to that detected for PE/α-MnO_2 nanocomposite. CI, HI, and NI data demonstrate that anatase TiO_2 is a photocatalyst of the last CO_2 cleavage stage. Interestingly, the PE photodegradation was enhanced by adding the composite filler (TiO_2&MnO_2) within the polymeric matrix. This coupling effect could be explained by considering that the combination with TiO_2 renders the MnO_2 nanoparticles more active in the first intermediate steps of PE oxidation. Consequently, the accumulation of the intermediates' functional groups is higher compared to the PE/TiO_2 film.

CRediT authorship contribution statement

Iryna Kovinchuk: Investigation, Data curation, Writing – original draft. **Nadiia Haiuk:** Investigation, Data curation. **Giuseppe Lazzara:** Conceptualization, Supervision. **Giuseppe Cavallaro:** Writing – review & editing, Validation. **Georgii Sokolsky:** Funding acquisition, Resources, Conceptualization, Supervision.

Declaration of Competing Interest

The authors declare that they have no known competing financial interests or personal relationships that could have appeared to influence the work reported in this paper.

Data availability

Data will be made available on request.

Acknowledgments

We acknowledge with Erasmus + Programme, Key Action 1 – Learning Mobility of Individuals, KA107 – Higher education, Grant Agreement No.2019–1-IT02-KA107–062108 between the University of Palermo and the Igor Sikorsky Kyiv Polytechnic Institute (Ukraine). We express our gratefulness to Maksym N. Zahornyi (Frantsevich Institute for Problems in Materials Science NA, Ukraine) for providing TiO_2 samples. The work was financially supported by FFR 2023

References

[1] R.-.D. Sun, T. Nishikawa, A. Nakajima, T. Watanabe, K. Hashimoto, TiO_2/polymer composite materials with reduced generation of toxic chemicals during and after combustion—Effect of HF-treated TiO_2, Polym. Degrad. Stab. 78 (2002) 479–484, https://doi.org/10.1016/S0141-3910(02)00191-X.

[2] D. Wang, P. Zhang, M. Yan, L. Jin, X. Du, F. Zhang, Q. Wang, B. Ni, C. Chen, Degradation mechanism and properties of debris of photocatalytically degradable plastics LDPE-TiO_2 vary with environments, Polym. Degrad. Stab. 195 (2022), 109806, https://doi.org/10.1016/j.polymdegradstab.2021.109806.

[3] S.S. Ali, I.A. Qazi, M. Arshad, Z. Khan, T.C. Voice, C.T. Mehmood, Photocatalytic degradation of low density polyethylene (LDPE) films using titania nanotubes, Environ. Nanotechnol. Monit. Manag. 5 (2016) 44–53, https://doi.org/10.1016/j.enmm.2016.01.001.

[4] M. Muscetta, S.A. Jitan, G. Palmisano, R. Andreozzi, R. Marotta, S. Cimino, I. D. Somma, Visible light – driven photocatalytic hydrogen production using Cu_2O/TiO_2 composites prepared by facile mechanochemical synthesis, J. Environ. Chem. Eng. 10 (2022), 107735, https://doi.org/10.1016/j.jece.2022.107735.

[5] S.Y. Lee, S.J. Park, TiO_2 photocatalyst for water treatment applications, J. Ind. Eng. Chem. 19 (2013) 1761–1769, https://doi.org/10.1016/j.jiec.2013.07.012.

[6] K. Maver, I. Arčon, M. Fanetti, S.A. Jitan, G. Palmisano, M. Valant, U.L. Štangar, Improved photocatalytic activity of SnO_2.TiO_2 nanocomposite thin films prepared by low-temperature sol-gel method, Catal. Today. 397–399 (2022) 540–549, https://doi.org/10.1016/j.cattod.2021.06.018.

[7] R.S. Dima, L. Phuthu, N.E. Maluta, J.K. Kirui, R.R. Maphanga, Electronic, structural, and optical properties of mono-doped and CO-doped (210) TiO_2 brookite surfaces for application in dye-sensitized solar cells—A first principles study, Materials (Basel) (2021) 14, https://doi.org/10.3390/ma14143918.

[8] M. Koelsch, S. Cassaignon, J.F. Guillemoles, J.P. Jolivet, Comparison of optical and electrochemical properties of anatase and brookite TiO_2 synthesized by the sol–gel method, Thin Solid Films 403–404 (2002) 312–319, https://doi.org/10.1016/S0040-6090(01)01509-7.

[9] F. Magalhães, F.C.C. Moura, R.M. Lago, TiO_2/LDPE composites: a new floating photocatalyst for solar degradation of organic contaminants, Desalination 276 (2011) 266–271, https://doi.org/10.1016/j.desal.2011.03.061.

[10] V.I. Shapovalov, Nanopowders and films of titanium oxide for photocatalysis: a review, Glass Phys. Chem. 36 (2010) 121–157, https://doi.org/10.1134/S108765961002001X.

[11] J.C. Tristão, F. Magalhães, P. Corio, M.T.C. Sansiviero, Electronic characterization and photocatalytic properties of CdS/TiO_2 semiconductor composite, J. Photochem. Photobiol. Chem. 181 (2006) 152–157, https://doi.org/10.1016/j.jphotochem.2005.11.018.

[12] A. Zielińska, E. Kowalska, J.W. Sobczak, I. Łącka, M. Gazda, B. Ohtani, J. Hupka, A. Zaleska, Silver-doped TiO_2 prepared by microemulsion method: surface properties, bio- and photoactivity, Sep. Purif. Technol. 72 (2010) 309–318, https://doi.org/10.1016/j.seppur.2010.03.002.

[13] M. Zhong, M. Li, Z. Fan, W. Huang, H. Hao, Z. Xia, Q. Zhang, H. Peng, Y. Zhang, Tuning the crystallinity of MnO_2 oxidant to achieve highly efficient pollutant degradation, Chin. Chem. Lett. 34 (2023), 107189, https://doi.org/10.1016/j.cclet.2022.01.082.

[14] N.D. Ivanova, S.V. Ivanov, E.I. Boldyrev, G.V. Sokol'skii, I.S. Makeeva, High-performance manganese oxide catalysts for CO oxidation, Russ. J. Appl. Chem. 75 (2002) 1420–1423, https://doi.org/10.1023/A:1022216626347.

[15] G. Liu, S. Liao, D. Zhu, J. Cui, W. Zhou, Solid-phase photocatalytic degradation of polyethylene film with manganese oxide OMS-2, Solid State Sci. 13 (2011) 88–94, https://doi.org/10.1016/j.solidstatesciences.2010.10.014.

[16] L. Zhang, D. He, P. Jiang, MnO_2-doped anatase TiO_2 – An excellent photocatalyst for degradation of organic contaminants in aqueous solution, Catal. Commun. 10 (2009) 1414–1416, https://doi.org/10.1016/j.catcom.2009.03.015.

[17] S. Taujale, H. Zhang, Impact of interactions between metal oxides to oxidative reactivity of manganese dioxide, Environ. Sci. Technol. 46 (2012) 2764–2771, https://doi.org/10.1021/es204294c.

[18] J.Q. Wei, X.J. Chen, P.F. Wang, Y.B. Han, J.C. Xu, B. Hong, H.X. Jin, D.F. Jin, X. L. Peng, J. Li, Y.T. Yang, H.L. Ge, X.Q. Wang, High surface area TiO2/SBA-15 nanocomposites: synthesis, microstructure and adsorption-enhanced photocatalysis, Chem. Phys. 510 (2018) 47–53, https://doi.org/10.1016/j.chemphys.2018.05.012.

[19] N.S. Allen, N. Mahdjoub, V. Vishnyakov, P.J. Kelly, R.J. Kriek, The effect of crystalline phase (anatase, brookite and rutile) and size on the photocatalytic activity of calcined polymorphic titanium dioxide (TiO2), Polym. Degrad. Stab. 150 (2018) 31–36, https://doi.org/10.1016/j.polymdegradstab.2018.02.008.

[20] A. Mills, S.L. Hunte, An overview of semiconductor photocatalysis, J. Photochem. Photobiol. Chem. 108 (1997) 1–35, https://doi.org/10.1016/S1010-6030(97)00118-4.

[21] J. Alvarado, G. Acosta, F. Perez, Study of the effect of the dispersion of functionalized nanoparticles TiO_2 with photocatalytic activity in LDPE, Polym. Degrad. Stab. 134 (2016) 376–382, https://doi.org/10.1016/j.polymdegradstab.2016.11.009.

[22] L. Lisuzzo, G. Cavallaro, S. Milioto, G. Lazzara, Halloysite nanotubes filled with MgO for paper reinforcement and deacidification, Appl. Clay Sci. 213 (2021), 106231, https://doi.org/10.1016/j.clay.2021.106231.

[23] S. Perinović Jozić, D. Jozić, M. Erceg, B. Andričić, S. Bernstorff, Nonisothermal crystallization of poly(l-lactide) in poly(l-lactide)/olive stone flour composites, Thermochim. Acta 683 (2020), 178440, https://doi.org/10.1016/j.tca.2019.178440.

[24] I. Kremer, T. Tomić, Z. Katančić, Z. Hrnjak-Murgić, M. Erceg, S. Vecchio Ciprioti, D.R. Schneider, Effect of zeolite catalyst on the pyrolysis kinetics of multi-layered plastic food packaging, Symmetry (Basel) (2022) 14, https://doi.org/10.3390/sym14071362.

[25] M.M. Calvino, L. Lisuzzo, G. Cavallaro, G. Lazzara, S. Milioto, Halloysite based geopolymers filled with wax microparticles as sustainable building materials with enhanced thermo-mechanical performances, J. Environ. Chem. Eng. 10 (2022), 108594, https://doi.org/10.1016/j.jece.2022.108594.

[26] K. Palaniandy, S.A.B. Auckloo, G. Cavallaro, E.S. Chan, P. Pasbakhsh, New insights into segmental packing, chain dynamics and thermomechanical performance of aliphatic polyurea composites: comparison between silica oxides and titanium (III) oxides, Macromol. Mater. Eng. 307 (2022), 2100582, https://doi.org/10.1002/mame.202100582.

[27] V.K. Mohonee, K.L. Goh, L. Mishnaevsky, P. Pasbakhsh, Capsule based self-healing composites: new insights on mechanical behaviour based on finite element analysis, Comput. Mater. Sci. 192 (2021), 110203, https://doi.org/10.1016/j.commatsci.2020.110203.

[28] I. Blanco, F.A. Bottino, G. Cicala, G. Ognibene, C. Tosto, Design, preparation and thermal characterization of polystyrene composites reinforced with novel three-cages POSS molecules, Molecules (2020) 25, https://doi.org/10.3390/molecules25132967.

[29] M. Catauro, G. Dal Poggetto, G. Cicala, L. Saitta, C. Tosto, I. Blanco, Thermo-oxidative investigation on SiO_2 and SiO_2–ZrO_2 composites prepared by sol–gel route, J. Therm. Anal. Calorim. 147 (2022) 5401–5412, https://doi.org/10.1007/s10973-021-11139-w.

[30] L. Botta, V. Titone, R. Teresi, M.C. Scarlata, G.L. Re, F.P.L. Mantia, F. Lopresti, Biocomposite PBAT/lignin blown films with enhanced photo-stability, Int. J. Biol. Macromol. 217 (2022) 161–170, https://doi.org/10.1016/j.ijbiomac.2022.07.048.

[31] G. Infurna, P.F. Teixeira, N.T. Dintcheva, L. Hilliou, F.P.L. Mantia, J.A. Covas, Taking advantage of the functional synergism between carbon nanotubes and graphene nanoplatelets to obtain polypropylene-based nanocomposites with enhanced oxidative resistance, Eur. Polym. J. 133 (2020), 109796, https://doi.org/10.1016/j.eurpolymj.2020.109796.

[32] G. Cavallaro, M.R. Caruso, S. Milioto, R. Fakhrullin, G. Lazzara, Keratin/alginate hybrid hydrogels filled with halloysite clay nanotubes for protective treatment of human hair, Int. J. Biol. Macromol. 222 (2022) 228–238, https://doi.org/10.1016/j.ijbiomac.2022.09.170.
[33] X. u Zhao, Z. Li, Y. Chen, L. Shi, Y. Zhu, Solid-phase photocatalytic degradation of polyethylene plastic under UV and solar light irradiation, J. Mol. Catal. Chem. 268 (2007) 101–106, https://doi.org/10.1016/j.molcata.2006.12.012.
[34] J. Almond, P. Sugumaar, M.N. Wenzel, G. Hill, C. Wallis, Determination of the carbonyl index of polyethylene and polypropylene using specified area under band methodology with ATR-FTIR spectroscopy, E Polymers 20 (2020) 369–381, https://doi.org/10.1515/epoly-2020-0041.
[35] G. Sokolsky, M.N. Zahornyi, T.F. Lobunets, N.I. Tyschenko, A. Shyrokov, A. V. Ragulya, S.V. Ivanov, N.V. Gayuk, V.E. Sokol'skii, Photoelectrocatalytic degradation of aminoazodyes of titanium dioxide with surface Ti^{3+} states, J. Chem. Technol. (2019) 130–139.
[36] S. Sahebian, S.M. Zebarjad, S.A. Sajjadi, Z. Sherafat, A. Lazzeri, Effect of both uncoated and coated calcium carbonate on fracture toughness of HDPE/$CaCO_3$ nanocomposites, J. Appl. Polym. Sci. 104 (2007) 3688–3694, https://doi.org/10.1002/app.25644.
[37] X. Tang, S. Alavi, Structure and physical properties of starch/poly vinyl alcohol/laponite RD nanocomposite films, J. Agric. Food Chem. 60 (2012) 1954–1962, https://doi.org/10.1021/jf2024962.
[38] T.G. Darshan, S. Veluri, B. Kartik, C. Yen-Hsiang, C. Fang-Chyou, Poly(butylene succinate)/high density polyethylene blend-based nanocomposites with enhanced physical properties – Selectively localized carbon nanotube in pseudo-double percolated structure, Polym. Degrad. Stab. 163 (2019) 185–194, https://doi.org/10.1016/j.polymdegradstab.2019.03.009.
[39] M.I. Tayouri, S. Estaji, S.R. Mousavi, S.S. Khasraghi, R. Jahanmardi, S. Nouranian, M. Arjmand, H.A. Khonakdar, Degradation of polymer nanocomposites filled with graphene oxide and reduced graphene oxide nanoparticles: a review of current status, Polym. Degrad. Stab. 206 (2022), 110179, https://doi.org/10.1016/j.polymdegradstab.2022.110179.
[40] S. Vyazovkin, A.K. Burnham, J.M. Criado, L.A. Pérez-Maqueda, C. Popescu, N. Sbirrazzuoli, ICTAC kinetics committee recommendations for performing kinetic computations on thermal analysis data, Thermochim. Acta 520 (2011) 1–19, https://doi.org/10.1016/j.tca.2011.03.034.
[41] O. Gutiérrez, H. Palza, Effect of carbon nanotubes on thermal pyrolysis of high density polyethylene and polypropylene, Polym. Degrad. Stab. 120 (2015) 122–134, https://doi.org/10.1016/j.polymdegradstab.2015.06.014.
[42] I. Blanco, L. Abate, M.L. Antonelli, F.A. Bottino, The regression of isothermal thermogravimetric data to evaluate degradation Ea values of polymers: a comparison with literature methods and an evaluation of lifetime predictions reliability. Part II, Polym. Degrad. Stab. 98 (2013) 2291–2296, https://doi.org/10.1016/j.polymdegradstab.2013.08.012.
[43] T. Saha, A.K. Bhowmick, T. Oda, T. Miyauchi, N. Fujii, Influence of layered nanofillers on the mechanical properties and thermal degradation of polyacrylicester polymer: theoretical and experimental investigations, Compos. Part B Eng. 169 (2019) 65–78, https://doi.org/10.1016/j.compositesb.2019.03.084.
[44] M.C. Celina, Review of polymer oxidation and its relationship with materials performance and lifetime prediction, Polym. Degrad. Stab. 98 (2013) 2419–2429, https://doi.org/10.1016/j.polymdegradstab.2013.06.024.
[45] E. Linde, N.H. Giron, M.C. Celina, Diffusion-limited hydrolysis in polymeric materials, Polym. Degrad. Stab. 204 (2022), 110095, https://doi.org/10.1016/j.polymdegradstab.2022.110095.
[46] L. Guadagno, C. Naddeo, V. Vittoria, G. Camino, C. Cagnani, Chemical and morphologial modifications of irradiated linear low density polyethylene (LLDPE), Polym. Degrad. Stab. 72 (2001) 175–186, https://doi.org/10.1016/S0141-3910(01)00024-6.
[47] L. Costa, M.P. Luda, L. Trossarelli, Ultra high molecular weight polyethylene—II. Thermal- and photo-oxidation, Polym. Degrad. Stab. 58 (1997) 41–54, https://doi.org/10.1016/S0141-3910(97)00010-4.
[48] W. Liang, Y. Luo, S. Song, X. Dong, X. Yu, High photocatalytic degradation activity of polyethylene containing polyacrylamide grafted TiO2, Polym. Degrad. Stab. 98 (2013) 1754–1761, https://doi.org/10.1016/j.polymdegradstab.2013.05.027.
[49] X. Zhao, Z. Li, Y. Chen, L. Shi, Y. Zhu, Enhancement of photocatalytic degradation of polyethylene plastic with CuPc modified TiO_2 photocatalyst under solar light irradiation, Appl. Surf. Sci. 254 (2008) 1825–1829, https://doi.org/10.1016/j.apsusc.2007.07.154.
[50] M.C. Celina, E. Linde, E. Martinez, Carbonyl identification and quantification uncertainties for oxidative polymer degradation, Polym. Degrad. Stab. 188 (2021), 109550, https://doi.org/10.1016/j.polymdegradstab.2021.109550.
[51] W.W. Focke, R.P. Mashele, N.S. Nhlapo, Stabilization of low-density polyethylene films containing metal stearates as photodegradants, J. Vinyl Addit. Technol. 17 (2011) 21–27, https://doi.org/10.1002/vnl.20248.
[52] M.C. Antunes, J.A.M. Agnelli, A.S. Babetto, B.C. Bonse, S.H.P. Bettini, Abiotic thermo-oxidative degradation of high density polyethylene: effect of manganese stearate concentration, Polym. Degrad. Stab. 143 (2017) 95–103, https://doi.org/10.1016/j.polymdegradstab.2017.06.012.
[53] A. Benítez, J.J. Sánchez, M.L. Arnal, A.J. Müller, O. Rodríguez, G. Morales, Abiotic degradation of LDPE and LLDPE formulated with a pro-oxidant additive, Polym. Degrad. Stab. 98 (2013) 490–501, https://doi.org/10.1016/j.polymdegradstab.2012.12.011.
[54] P.J. Van Der Put, Solid state reactions. Inorg. Chem. Mater. Make Things Elem., Springer US, Boston, MA, 1998, pp. 167–190, https://doi.org/10.1007/978-1-4899-0095-1_5.